

The role of non-normality in overreflection theory

Nikolaos A. Bakas*

Brian F. Farrell

Harvard University

Harvard University

Cambridge, MA 02138

Cambridge, MA 02138

March 24, 2010

Submitted to the Journal of Atmospheric Sciences

*corresponding author : Nikolaos Bakas, National and Kapositrian University of Athens, Build. IV, office 34, Panepistimiopolis, Zografos, Athens, Greece, email: nbakas@post.harvard.edu

ABSTRACT

The role of non-normality in the overreflection of gravity waves is investigated. In the limit of weak stratification, wave packets having a critical level inside a shear layer of finite depth are reflected with amplified energy. This process, which exhibits the characteristics of stimulated emission, occurs in three stages: first the incoming wave enters the shear layer and excites non-propagating perturbations leaning towards and against the shear. Subsequently, the energy of perturbations leaning against the shear grows in a manner similar to energy growth of perturbations in constant shear flows, indicating that the Orr mechanism that is slightly modified by stratification underlies the observed growth. Finally, the amplified perturbations excite propagating waves originating from the vicinity of the shear layer boundary. The role of non-normality in this process is also investigated from the perspective of the associated non-orthogonality of the modes of the dynamical system. It is found that the incident wave packet projects on non-orthogonal analytic modes having the structure of a downward propagating wave in the far field below the shear layer and overreflection results from the interaction among these non-orthogonal modes.

1. Introduction

Shear instability of stably stratified fluids is a common feature of atmospheric and oceanic flows that has been studied for over a century. However, despite the fact that the conditions under which shear instability occurs are now well known, the physical mechanism underlying the instability is not comprehensively understood. Conceptual frameworks that have been advanced for a physical, mechanistic basis for shear instability are the overreflection theory and the counter-propagating Rossby wave theory.

Overreflection theory (see Lindzen (1988) for a review) describes the instability of stably stratified flows in terms of continuous overreflection of gravity waves. Overreflection is a process initially noted by Jones (1968) who studied the scattering properties of a shear region with Richardson number less than $1/4$. Jones (1968) found that a gravity wave propagating towards a critical level embedded in a shear region is overreflected (that is the reflection coefficient exceeds one) due to extraction of energy from the mean flow. Lindzen (1974) further suggested that if the overreflected waves were fully reflected back by a containing surface and if the fully reflected and overreflected waves interfered constructively (by satisfying a proper quantization condition), then every time they traveled across the region between the overreflecting critical level and the containing surface, they would be amplified by the same factor and by being continuously overreflected, they could lead to the formation of an exponentially growing eigenmode. Lindzen and Rosenthal (1976, 1981, 1983), Rosenthal and Lindzen (1983a,b) and Lindzen and Tung (1978) found the necessary conditions for overreflection and for quantization of the waves and were able to relate all unstable modes with continuously overreflected waves in the cases of barotropic, baroclinic and stratified shear flow instabilities. Hence, shear flow instability appears

to be closely related to the overreflection process.

In order to shed more light on the mechanism of overreflection, Lindzen and Barker (1985) studied the time evolution of the scattering of an incident wave train under a specific wave geometry and found that the reflected and transmitted wave amplitudes at steady state are equal and that the characteristic time scale needed for the reflected and transmitted wave amplitudes to reach their steady state values is almost identical. This result is consistent with overreflection being a stimulated emission instigated by the incident wave. Lindzen and Barker (1985) also found that this characteristic time scale depended only on the variation of velocity across the critical level and was independent of the Richardson number in the vicinity of this level. This indicated that the stimulated emission is a kinematic effect. Based on this result, Lindzen (1988) hypothesized that the Orr mechanism (Orr 1907), in which a perturbation leaning against the shear intensifies transiently as it is sheared over, provides the necessary energy extraction mechanism from the mean flow in the process of overreflection. However, he did not support this hypothesis with numerical or analytical evidence. Transient growth of small perturbations in stratified flows was investigated by Farrell and Ioannou (1993) who were able to identify the Orr mechanism, that was slightly modified by stratification, as the underlying mechanism for rapid transient perturbation growth. Farrell and Ioannou (1993) also traced the observed energy growth to the non-normality of the dynamical operator governing the perturbation dynamics. However, since their analysis was performed for a flow lacking the wave geometry for overreflection (Lindzen 1988), these results do not directly apply to perturbation growth during overreflection. In this work we undertake this task to study the scattering of a wave packet by a finite stably stratified shear layer bounded by two regions of uniform velocity and clarify the role of non-normality and the Orr mechanism in the overreflection process.

A very different approach to understanding modal instability is through the framework of counter propagating Rossby waves that was pioneered by Bretherton (1966a) for Rossby waves. Bretherton (1966a) showed that unstable modes can be associated with a constructive interaction between two counter propagating Rossby edge waves that become phase locked in a mutual reinforcing configuration. This approach of interacting edge waves that are supported by regions of vorticity or density gradient discontinuity was followed by studies of baroclinic (Hoskins et al. 1985; Davies and Bishop 1994), Kelvin-Rossby wave (Sakai 1989), planar shear flow (Heifetz and Methven 2005) and Holmboe instabilities (Baines and Mitsudera 1994). In addition to application of the counter-propagating Rossby wave idea to models in which vorticity or density gradient discontinuities support edge waves which addresses the corresponding normal modes of the discrete spectrum, Heifetz and Methven (2005) extended Bretherton’s formulation to include the continuous spectrum and developed a generalized form of counter-propagating Rossby wave theory describing the complete spectrum solutions in terms of kernel-wave interactions. Harnik and Heifetz (2007) used this kernel formulation to show that overreflection in the case of barotropic instability can be understood as a mutual amplification of kernel Rossby waves, therefore relating the theories of overreflection and counter propagating Rossby waves. A similar kernel-wave formulation has been developed recently for stratified flows (Harnik et al. 2008) but has not been applied yet to the overreflection of gravity waves.

Since overreflection involves transient algebraic growth rather than exponential growth of perturbations, a comprehensive understanding of this process requires the methods of Generalized Stability Theory (GST; Farrell and Ioannou (1996)) which extends modal stability theory to account for all growth processes. In this work, we apply the tools of GST to study the overreflection of a gravity wave packet by a stably stratified shear layer of finite depth. Our focus is

on the role of non-normal interactions among the analytic modes of the system in overreflection. The overall goal is to provide new insight into this process that will deepen our mechanistic understanding of shear instability.

This paper is organized as follows. Section 2 describes the evolution equations for perturbations in a stably stratified flow. In section 3 we review the necessary conditions for overreflection by studying the scattering of a monochromatic wave by a shear layer. In section 4 we elaborate on the transient characteristics of overreflection and study the scattering of a gravity wave packet by a shear layer of finite depth focusing on the energetics and propagation properties involved. In section 5 we trace the overreflection process to non-normal excitation of the analytic modes of the dynamical system and we finally end with a brief discussion and our conclusions in section 6.

2. Evolution equations for a two dimensional stratified flow

Consider a flow with mean zonal velocity $U(z)$ varying in the vertical direction in a Boussinesq fluid with background density $\rho_0(z)$ varying with height. Small perturbations of zonal, u_ϵ , and vertical, w_ϵ , velocities as well as density, ρ_ϵ , and pressure, p_ϵ , perturbations are superposed on the mean fields. The evolution of harmonic perturbations of the form

$$(u_\epsilon(x, z, t), w_\epsilon(x, z, t), p_\epsilon(x, z, t), \rho_\epsilon(x, z, t)) = (\tilde{u}(z, t), \tilde{w}(z, t), \tilde{p}(z, t), \tilde{\rho}(z, t)) e^{ikx},$$

where k is the zonal wavenumber, is governed by the linearized, nondimensional equations:

$$(\partial_t + ikU(z))u + w \frac{dU}{dz} = -ikp - r(z)u + \frac{1}{\text{Re}} \nabla^2 u, \quad (1)$$

$$(\partial_t + ikU(z))w = -\partial_z p - \text{Ri}\rho - r(z)w + \frac{1}{\text{Re}} \nabla^2 w, \quad (2)$$

$$(\partial_t + ikU(z))\rho = w - r(z)\rho + \frac{1}{\text{Re}} \nabla^2 \rho, \quad (3)$$

$$iku + \partial_z w = 0, \quad (4)$$

where the following nondimensionalizations have been made:

$$\tilde{t} = (1/\alpha)t, \quad (\tilde{x}, \tilde{z}) = (V_0/\alpha)(x, y), \quad (\tilde{u}, \tilde{w}) = V_0(u, w), \quad \tilde{p} = \rho_m V_0^2 p, \quad \tilde{\rho} = (\rho_m V_0 N_0^2 / \alpha g)\rho,$$

in which the tilde denotes dimensional variables, α is the shear, V_0 , ρ_m are typical values for mean flow velocity and density and g is the gravitational acceleration. The Richardson and Reynolds numbers are defined as $\text{Ri} = N_0^2/\alpha^2$ and $\text{Re} = LV_0/\nu$ respectively, where ν is the coefficient of kinematic viscosity that has been chosen to be equal to the coefficient of density diffusion and N_0 is a typical value of the Brunt- Väisälä frequency such that $N_0^2 = -(g/\rho_m)(d\rho_0/dz)$. The Rayleigh damping $r(z)$ terms are introduced to allow for sponge layers in the numerical calculations presented in sections 4 and 5 where further details will be provided.

The system (1)-(4) can be reduced by taking the curl of (1)- (2) and expressing the perturbation velocity field in terms of a streamfunction $(u, w) = (\psi_z, -ik\psi)$ such that u, w satisfy (4), to finally obtain two equations for the perturbation streamfunction, ψ , and density, ρ :

$$(\partial_t + ikU(z) + r(z))(\nabla^2 \psi) - ik\psi \frac{d^2 U}{dz^2} = -\frac{dr}{dz} \partial_z \psi + ik\text{Ri}\rho + \frac{1}{\text{Re}} \nabla^4 \psi, \quad (5)$$

$$(\partial_t + ikU(z) + r(z))\rho + ik\psi = \frac{1}{\text{Re}}\nabla^2\rho, \quad (6)$$

where $\nabla^2 = d^2/dz^2 - k^2$ and $\nabla^4 = (\nabla^2)^2$.

3. Scattering of a monochromatic gravity wave by a shear layer

In this section, we review the necessary conditions for overreflection by studying the scattering of a monochromatic wave by a shear layer. Closed form solutions can be obtained in the absence of viscosity for the piecewise continuous mean flow profile

$$U(z) = \begin{cases} V_0, & \text{for } z > H/2 \\ 2V_0z/H, & \text{for } |z| \leq H/2 \\ -V_0, & \text{for } z \leq -H/2 \end{cases}, \quad (7)$$

that is shown in Fig. 1. It consists of a localized shear layer bounded by two regions of uniform velocity. Values of length and time used in nondimensionalization are the shear region width $H = 2$ and the inverse shear $1/\alpha = H/2V_0 = 1$.

Harmonic functions of the form $[\psi, \rho] = [\hat{\psi}(z), \hat{\rho}(z)]e^{-ikct}$ satisfying (5)-(6) with $r(z) = 0$ solve:

$$\frac{d^2\hat{\psi}}{dz^2} + \left(\frac{\text{Ri}}{(U(z) - c)^2} - \frac{d^2U}{dz^2} \frac{1}{(U(z) - c)} - k^2 \right) \hat{\psi} = 0. \quad (8)$$

The solution of (8) is :

$$\hat{\psi}(z, c) = \begin{cases} T e^{im_t(z-H/2)}, \text{ for } z \geq H/2 \\ C \sqrt{k(z-c)} I_\mu(k(z-c)) + D \sqrt{k(z-c)} I_{-\mu}(k(z-c)), \text{ for } |z| < H/2 \\ e^{-im(z+H/2)} + R e^{im(z+H/2)}, \text{ for } z \leq -H/2 \end{cases} \quad (9)$$

where m_t and m are the square root of $\text{Ri}/(V_0 - c)^2 - k^2$, $\mu = \sqrt{1/4 - \text{Ri}}$ and $I_{\pm\mu}$ is the modified Bessel function of the second kind of order μ . If we seek bounded solutions or impose radiation conditions at infinity, then m_t and m satisfy the conditions $\Re(m_t)(\Re(c) - V_0) < 0$, $\Im(m_t) > 0$ and $\Re(m)\Re(c) > 0$, $\Im(m) < 0$, where \Re and \Im denote the real and imaginary part respectively. The incident wave ($\exp(-im(z + H/2))$) has a unit amplitude, while the amplitudes of the reflected R , and the transmitted T waves for a given phase speed c are obtained in Appendix A.

Previous studies have shown that overreflection occurs in the following cases: in the first case, \mathbf{A} has a neutral mode having the structure of a propagating wave in the far field. An incident wave having the same phase speed as the neutral mode resonates with the mode, producing a reflected wave amplitude that grows as the integral of the incident wave (McIntyre and Weissman 1978). In the second case, \mathbf{A} does not have neutral or unstable radiating modes and overreflection occurs due to extraction of energy from the shear flow (Lindzen 1988). In this work we focus on the latter case, for which the following conditions are necessary for the occurrence of overreflection (Lindzen 1988): the first condition is that the incident wave should have a critical level within the shear region and that the Richardson number in the vicinity of the critical level should be $\text{Ri} < 1/4$. The second condition is the existence of a trapping region below the critical level, where the wave decays exponentially, so that the wave can tunnel through this region and reach the critical level in finite time, rather than approach the critical level asymptotically with ever decreasing group velocity as predicted by WKB analysis

(Bretherton 1966b). The third condition is the existence of a sink for wave flux on the side of the critical level opposite to the side of the wave region. This sink can be a second wave region or even a friction layer. Choosing $\text{Ri} = 0.2$, $k = 0.275$ and $m = -3$ satisfies all of the above conditions as the incident wave has a critical level at $z = c = -0.85$ for which the Richardson number is less than $1/4$. Also, close to the critical level the wave decays exponentially as the solution to (8) is well approximated for $|z - c| \ll 1$ by:

$$\hat{\psi}(z, c) \simeq C \exp\left(\sqrt{1/4 - \text{Ri}} \log(z - c)\right) + D \exp\left(-\sqrt{1/4 - \text{Ri}} \log(z - c)\right),$$

and above the critical level there is a small region of wave propagation that acts as a sink of wave flux. Calculation of the reflection coefficient verified the occurrence of overreflection, with $R = 1.5$. In addition, calculation of the discrete spectrum of \mathbf{A} in Appendix A, showed that for these values of k, Ri there are no modal solutions. For this range of values, the spectrum of \mathbf{A} consists only of a real number infinity of non-orthogonal, singular neutral modes forming a continuous spectrum (Case 1960). Therefore overreflection must result from the non-normal interaction among these singular modes. In the next sections we elaborate on the transient characteristics of the overreflection process and on the role of non-normality by studying the scattering of a wavepacket with the same central wavenumber as the monochromatic wave in this section.

4. Scattering of a gravity wave packet by a shear layer

Consider the scattering of a wave packet by a finite stably stratified shear layer with mean velocity profile :

$$U(z) = \begin{cases} 2V_0z/H, & 0 \leq |z| < \frac{H-z_w}{2} \\ \text{sgn}(z)V_0 - \text{sgn}(z)z_w f\left(\frac{z_w+H-2|z|}{2z_w}\right), & \frac{H-z_w}{2} \leq |z| < \frac{H+z_w}{2} \\ \text{sgn}(z)V_0, & |z| \geq \frac{H+z_w}{2} \end{cases}, \quad (10)$$

where

$$f(x) = \begin{cases} \frac{2}{3}x^3, & 0 \leq x < \frac{1}{2} \\ -\frac{2}{3}x^3 + 2x^2 - x + \frac{1}{6}, & \frac{1}{2} \leq x < 1 \end{cases}.$$

This profile differs from profile (7) only within a region of width $z_w = 0.2$ at the boundaries of the shear layer, where in this case the corners are rounded (c.f Fig. 1). The initial perturbation is of the form $[\psi_0(z), \rho_0(z)]e^{ikx}$ and is localized in the lower region of uniform velocity. It can be readily shown that in the absence of viscosity and damping this perturbation initially propagates in the region of uniform velocity according to :

$$[\psi(x, z, t), \rho(x, z, t)] = \frac{1}{\sqrt{2\pi}} \int_{-\infty}^{\infty} [\hat{\psi}(m, t), \hat{\rho}(m, t)] e^{ikx+imz} dm, \quad (11)$$

where

$$\hat{\psi}(m, t) = \frac{1}{2} \left(\hat{\psi}_0(m) - c\hat{\rho}_0(m) \right) e^{ik(-V_0+c)t} + \frac{1}{2} \left(\hat{\psi}_0(m) + c\hat{\rho}_0(m) \right) e^{ik(-V_0-c)t}, \quad (12)$$

$\hat{\rho}(m, t) = -(i/kc^2)(d\hat{\psi}/dt) - V_0\hat{\psi}/c^2$ and

$$[\hat{\psi}_0(m), \hat{\rho}_0(m)] = \frac{1}{\sqrt{2\pi}} \int_{-\infty}^{\infty} [\psi_0(z), \rho_0(z)] e^{-imz} dz,$$

are the Fourier components of the initial perturbation. The two terms in (12) correspond to two counter-propagating gravity waves with phase speed $c = \sqrt{\text{Ri}}/\sqrt{k^2 + m^2}$. We launch a localized

wavepacket with initial density:

$$\rho_0(z) = \Gamma e^{im_0 z} e^{-((z-z_0)^2/\delta z)^2}, \quad (13)$$

where $(k, m_0) = (0.275, -3)$, $\delta z = 2$, $z_0 = -5.5$ and Γ is a chosen amplitude yielding unit initial energy. The initial streamfunction

$$\psi_0(z) = \frac{\Gamma \delta z \sqrt{\text{Re}} e^{-im_0 z_0}}{2\sqrt{\pi}} \int_{-\infty}^{\infty} \frac{1}{\sqrt{k^2 + m^2}} e^{im(z_0-z)} e^{-(m-m_0)^2(\delta z)^2/4} dm, \quad (14)$$

is chosen so that the first term in (12) is zero for all wavenumbers. As a result the initial perturbation comprising of a narrow spread of wavenumbers around $m_0 = -3$ propagates upwards as a coherent wave packet with group velocity $c_g = -km_0\sqrt{\text{Re}}/(k^2 + m_0^2)^{3/2}$.

We numerically obtain the time evolution of the initial perturbation by first rewriting (5)-(6) in the compact form:

$$\frac{d\mathbf{x}}{dt} = \mathbf{A}\mathbf{x}, \quad (15)$$

where $\mathbf{x}(t) = [\psi(t), \rho(t)]^T$ is the state vector and

$$\mathbf{A} = \begin{pmatrix} \nabla^{-2} \left(-(ikU + r)\nabla^2 + ik\frac{d^2U}{dz^2} - \frac{dr}{dz}\partial_z + \frac{1}{\text{Re}}\nabla^4 \right) & ik\text{Re}\nabla^{-2} \\ -ik & -(ikU + r) + \frac{1}{\text{Re}}\nabla^2 \end{pmatrix}, \quad (16)$$

is the dynamical operator. We then discretize the differential operators in (16), incorporating the appropriate boundary conditions (zero streamfunction and zero momentum and thermal fluxes at the boundaries), and interpret (15) as a matrix equation in which the state becomes a column vector. We also impose radiation conditions at infinity by inserting sponge layers at the top and bottom of the domain with Rayleigh friction coefficient:

$$r(z) = a_r(1 + \tanh((z - z_p)/\delta_r)) + a_r(1 - \tanh((z + z_p)/\delta_r)),$$

in which a_r is the damping amplitude, z_p determines the vertical position of the sponges and δ_r determines the transition width into the sponge layer. Numerical tests showed no spurious back-reflection either from the upper and lower boundaries or from variation of $r(z)$. Finally, a small amount of diffusion ($\text{Re} = 10^6$) is also introduced to serve as a sink for energy transferred to unresolved scales in the vicinity of the critical level due to the rapid increase of the wave's vertical wavenumber in this region.

The time evolution of this localized perturbation obtained by numerical integration of (15) is illustrated in Fig. 2, where contours of streamfunction perturbation at successive times are shown. The initial wave packet (Fig. 2a) propagates upwards and its initial evolution follows closely (11) as revealed by comparison of the numerical solution with (11). As it enters the shear region it excites perturbations with phase lines leaning towards and against the shear resulting in the vertically tilted structure shown in Fig. 2b. It is worth noting that immediately after the wave packet enters the shear layer, the density perturbations are confined below the critical layer of the wave packet (not shown), as would be expected for a wave propagating towards its critical level. However, the streamfunction perturbations occupy the whole shear region (Fig. 2b), showing that the excitation of the streamfunction within the shear region is non-local. This non-local excitation is an indication of wave-tunneling through the critical level that is merely assured by the condition of $\text{Ri} < 1/4$ as discussed in the previous section. Perturbations leaning against the shear do not propagate vertically for such low Richardson numbers (Hartman 1975). They grow in place and excite vertically propagating disturbances originating from the region of the shear layer corners as shown in Fig. 2c. These disturbances subsequently propagate downward as a coherent wave packet (Fig. 2d). The non-local character of the excitation of the streamfunction inside the shear layer, along with the fact that the downward propagating

waves originate from the vicinity of the shear layer corners rather than from the vicinity of the critical layer indicates that the reflection process has the characteristics of an emission that is stimulated by the incident wave packet in agreement with the transient evolution results of Lindzen and Barker (1985). Evolution of perturbation energy is calculated as

$$E = \int \left(\frac{1}{4} \overline{u^2} + \frac{1}{4} \overline{w^2} + \frac{\text{Ri}}{4} \overline{\rho^2} \right) dz = \mathbf{x}^\dagger \mathbf{M} \mathbf{x}, \quad (17)$$

where the overbar denotes an average in the zonal direction, \dagger denotes the complex conjugate and

$$\mathbf{M} = \frac{\Delta z}{4} \begin{pmatrix} -d^2/dz^2 + k^2 & 0 \\ 0 & \text{Ri} \end{pmatrix},$$

is the energy metric with grid interval Δz . Figure 3a showing the evolution of perturbation energy in the lower region illustrates that the downward propagating wave packet (Fig. 2d) has more energy than the initial wave packet. Additional evidence for overreflection of the incident wave packet was found by a Fourier decomposition of the reflected packet that yielded

$$|\hat{\psi}_r(-m_0)| = 1.5 |\hat{\psi}_i(m_0)|,$$

where $\hat{\psi}_r, \hat{\psi}_i$ are the Fourier amplitudes for the reflected and the incident wavepacket respectively. Since the reflected Fourier amplitude calculated at the central wavenumber coincides with the reflected amplitude of the monochromatic wave with the same wavenumber, we conclude that there is a one to one correspondence between the transient wavepacket reflection and the steady state scattering problem. Summarizing, the scattering of the wave packet by the shear layer has the characteristics of stimulated emission and can be separated into three stages : non-local excitation of perturbations that do not propagate in the vertical within the shear layer by the velocity component of the incident wave, which occurs as the incident wave tunnels through

the region of the critical level; growth of the excited perturbations within the shear region; and excitation by these amplified perturbations of vertically propagating waves.

We now focus on perturbation growth within the shear region. Transient growth of perturbations in a stably stratified, constant shear flow was studied by Farrell and Ioannou (1993) who found that for low Richardson numbers perturbation vorticity is conserved for early times. Kinematic deformation of vorticity by the shear flow leads to substantial growth of velocity perturbations as first discussed by Kelvin (1887) and Orr (1907) with the downgradient Reynolds stresses being the mechanism of energy exchange between the mean flow and the perturbations. They also found that the Orr mechanism is modified by stratification, as buoyancy fluxes convert kinetic energy into potential energy and limit the overall energy growth compared to the unstratified case. The finite time required for this energy conversion results in a time lag between kinetic and potential energy growth, with the potential energy peak lagging behind the kinetic energy peak. To investigate whether the Orr mechanism is associated with perturbation growth in the shear region during overreflection, we calculated the kinetic and potential energy within the shear region by using the norms

$$\mathbf{M}_{\mathbf{k}} = \frac{\Delta z}{4} \begin{pmatrix} -d^2/dz^2 + k^2 & 0 \\ 0 & 0 \end{pmatrix},$$

$$\mathbf{M}_{\mathbf{p}} = \frac{\Delta z}{4} \begin{pmatrix} 0 & 0 \\ 0 & \text{Ri} \end{pmatrix},$$

expressing perturbation kinetic and potential energy in terms of the Euclidean inner products

$$E_k = \int_{-H/2}^{H/2} \left(\frac{1}{4} \overline{u^2} + \frac{1}{4} \overline{w^2} \right) dz = \mathbf{x}^\dagger \mathbf{M}_{\mathbf{t}} \mathbf{M}_{\mathbf{k}} \mathbf{x}, \quad (18)$$

and

$$E_p = \int_{-H/2}^{H/2} \left(\frac{\text{Ri}}{4} \overline{\rho^2} \right) dz = \mathbf{x}^\dagger \mathbf{M}_t \mathbf{M}_p \mathbf{x}, \quad (19)$$

respectively. The projection matrix $\mathbf{M}_t = \text{diag}(0 \ 0 \dots 0 \ 0 \ 1 \ 1 \dots 1 \ 1 \ 0 \ 0 \dots 0)$ with ones only at the grid points that are inside the shear region, merely imposes the domain of integration. We also calculated the average Reynolds stress and buoyancy fluxes within the shear region:

$$\langle \overline{uw} \rangle = \frac{1}{2} \int_{-H/2}^{H/2} \overline{uw} dz = \frac{\Delta z}{4} \mathbf{x}^\dagger \mathbf{W}^\dagger \mathbf{M}_t \mathbf{U} \mathbf{x}, \quad (20)$$

and

$$\langle \overline{\rho w} \rangle = \frac{1}{2} \int_{-H/2}^{H/2} \overline{\rho w} dz = \frac{\Delta z}{4} \mathbf{x}^\dagger \mathbf{W}^\dagger \mathbf{M}_t \mathbf{P} \mathbf{x}, \quad (21)$$

where \mathbf{U} , \mathbf{W} , \mathbf{P} are projection matrices giving u , w , ρ in terms of the state vector \mathbf{x} respectively ($\mathbf{u} = \mathbf{U}\mathbf{x}$, $\mathbf{w} = \mathbf{W}\mathbf{x}$, $\rho = \mathbf{P}\mathbf{x}$). As shown in Fig. 3b, there is an initial increase in kinetic energy that can be traced to the downgradient Reynolds stresses shown in Fig. 3c. The kinetic energy amplification is redistributed through the positive buoyancy fluxes shown in Fig. 3d to potential energy lagging behind kinetic energy by 30 advection time units as illustrated in Fig. 3c. Therefore, perturbation growth inside the shear region during overreflection exhibits the same characteristics found by Farrell and Ioannou (1993) in their study of transient growth in a constant shear flow. This is a strong indication that the modified Orr mechanism underlies perturbation growth during overreflection. The role of non-normality and mode interaction in producing the observed growth will now be further investigated.

5. Stimulated emission as excitation of the continuous spectrum modes

In this section we relate the stimulated emission to non-normal excitation of the analytic modes of the dynamical operator. We first express (15) in terms of a new variable $\mathbf{y} = \mathbf{M}^{1/2}\mathbf{x}$ for which the energy is given by the Euclidian product $E = \mathbf{y}^\dagger\mathbf{y}$. Perturbation evolution can then be written in terms of the new dynamical operator $\mathbf{D} = \mathbf{M}^{1/2}\mathbf{A}\mathbf{M}^{-1/2}$ as :

$$\frac{d\mathbf{y}}{dt} = \mathbf{D}\mathbf{y}.$$

As discussed in section 3, the spectrum of \mathbf{D} consists in the inviscid case of a continuous spectrum of singular neutral modes. In the presence of diffusion however small, the singular neutral modes are replaced by a set of analytic, non-orthogonal modes. The dispersion relation of the analytic modes for $k = 0.275$, $\text{Ri} = 0.2$ and $\text{Re} = 10^3$ is shown in Fig. 4. The spectrum consists of a “Y” shaped branch, hereafter shear branch, resembling the unstratified shear flow spectrum (Dongarra et al. 1996), and two branches, hereafter scattering branches, containing a large number of modes with phase speeds close to $c = \pm V_0 = \pm 1$. The shear modes are localized within the shear layer as shown in Fig. 5a and resemble the analytic modes of unstratified flow (Reddy et al. 1993). On the other hand the scattering modes are not localized and have a wavelike structure in the far field as illustrated in Fig. 5b. The scattering modes corresponding to different eigenvalues have different vertical wavelength in the far field, with the modes having longer wavelengths occupying the upper part of the spectrum (that is they correspond to eigenvalues with small negative real part) as expected for diffusive dissipation.

Evolution of an initial perturbation $\mathbf{y}(0)$ can now be expressed as an expansion in the com-

plete basis of the normalized eigenmodes \mathbf{u}_i as

$$\mathbf{y}(t) = \sum_i a_i e^{i\omega_i t} \mathbf{u}_i, \quad (22)$$

where ω_i are the eigenvalues corresponding to \mathbf{u}_i and a_i are the corresponding projection coefficients. The projection coefficients can be calculated as

$$a_i = \frac{(\mathbf{v}_i, \mathbf{y}(0))}{(\mathbf{v}_i, \mathbf{u}_i)}, \quad (23)$$

where \mathbf{v}_i are the eigenvectors of the adjoint matrix \mathbf{D}^\dagger that are biorthogonal to the normal modes of \mathbf{D} (Farrell and Ioannou 1996). Using (23) we calculate the projection coefficients for the initial wavepacket given by (13)-(14). By comparing the wave packet evolution given by (22) to the evolution obtained by numerical integration of (15), we find that a small subset of only 30 members of the scattering branch modes having similar structure is adequate to describe the reflected wave packet. A member of this subset is plotted in Fig. 6a. The lower part of the mode (lying approximately below $z = -H/2 = -1$) has the structure of a wave leaning against the shear. Fourier decomposition of the lower part of the mode shown in Fig. 6b reveals that the mode has the form of a wave consisting mainly of positive vertical wavenumbers. The upper part (lying approximately above $z = H/2 = 1$) decays exponentially away from the shear region. We therefore do not expect to find our initial perturbation propagating upwards away from the shear flow. This result is consistent with the steady state result of Lindzen and Rosenthal (1981) and Eltayeb and McKenzie (1975) who found overreflected waves propagating both above and below the critical layer only for $\text{Ri} < 0.1146$.

Projection of the initial perturbation onto the spectrum of the dynamical operator reveals two further results worth noting: the first is that at no time does the wave packet look like any of these modes individually as would be the case of an unstable mode dominating after a

long time. It is the sum over this subset of modes forming the perturbation and the nonnormal interaction among them that produces the observed growth. This underscores the essential non-normal nature of the overreflection process. The second is that the initial perturbation (leaning against the shear and propagating energy upwards c.f. Fig. 2a) does not appear at first glance to project on the modes shown in Fig. 6a (leaning with the shear in the lower region of uniform velocity and propagating energy downwards). But for nonnormal systems, the perturbation with the maximum projection on a certain mode is the complex conjugate of the adjoint mode (Farrell and Ioannou 1996). Fig. 6c shows the complex conjugate of the adjoint mode plotted in Fig. 6a. Fourier decomposition of the lower part of the adjoint mode plotted in Fig. 6d clearly illustrates that the initial perturbation (wave packet centered at $m_0 = -3$) does indeed project most strongly on the mode in Fig. 6a.

6. Conclusions

In this paper we examined the role of non-normality in the overreflection process. Initially the scattering of a monochromatic gravity wave by a finite shear layer was investigated using closed form solutions and the conditions under which overreflection occurs were reviewed. The scattering of a gravity wave packet by a shear layer was subsequently investigated focusing on the transient characteristics of the overreflection process. It was found that for $\text{Ri} < 1/4$, wave packets having a critical level inside the shear region are reflected with amplified energy. It was also shown that the process of overreflection occurs in three stages: during the first stage, the incoming wave enters the shear layer, tunnels through the critical level and excites perturbations that do not propagate in the vertical. The excitation is non-local as a result of the tunneling

of the wave and the streamfunction perturbations occupy the whole shear region. During the second stage, the energy of the non-propagating perturbations grows and during the final stage the amplified perturbations excite propagating waves in the far field originating from the vicinity of the shear layer boundary. These results therefore were found to support the conclusion of Lindzen and Barker (1985) that overreflection has the characteristics of stimulated emission.

Perturbation energy amplification during the second stage was further investigated. It was found that the kinetic energy of perturbations is amplified due to downgradient Reynolds stresses and a part of the amplified kinetic energy is converted to potential energy through positive buoyancy fluxes. Due to the finite time required for conversion, potential energy growth was found to lag behind kinetic energy growth. These results that are common of perturbation growth in stratified shear flows with low Richardson number (Farrell and Ioannou 1993) indicate that the modified Orr mechanism (Farrell and Ioannou 1993) produces the observed growth during overreflection and reveals the essential non-normality underlying the overreflection process. This result is also in agreement with the conclusion of (Harnik and Heifetz 2007) that the Orr mechanism underlies perturbation growth in the overreflection of Rossby waves, while the role of the kernel–wave interactions is to hold the perturbation at a configuration that is favorable for energy growth.

Finally, the link between overreflection and nonnormal interaction between the analytic modes of the dynamical system was highlighted. Eigenanalysis of the linear, viscous dynamical operator revealed a finite number of non-orthogonal, analytic modes replacing the non-orthogonal singular modes of the operator in the inviscid case. It was shown that reflection occurs as the incident wave packet projects strongly on the modes of the spectrum having the structure of a downward propagating wave in the far field below the shear layer, while the excess

energy of the reflected wave is traced to the non-normal interaction among these modes.

Acknowledgments

This research was supported by NSF ATM-0736022. Nikos Bakas would like to thank Prof. Richard Lindzen for introducing the problem of overreflection and fruitful discussions on an early version of the paper and Petros Ioannou for fruitful discussions. The authors would also like to thank two anonymous reviewers for their comments which helped improve the manuscript.

APPENDIX

Calculation of the discrete spectrum for an inviscid shear layer and closed form solution for the scattering of a monochromatic wave

In order to find the amplitudes R, C, D, T in (9), we apply continuity of displacement and pressure at $z = \pm H/2$ (implying continuity of $\hat{\psi}/(U(z) - c)$ and $(U(z) - c)d\hat{\psi}/dz - \hat{\psi}dU/dz$ at $z = \pm H/2$ respectively) to obtain the following equation:

$$\mathbf{B}(c)\mathbf{Y} = [1, 0, 0, 0]^T, \quad (\text{A1})$$

where $\mathbf{Y} = [R, C, D, T]^T$ and

$$\mathbf{B}(c) = \begin{pmatrix} 1 & -a_+ & -a_- & 0 \\ -im(H/2 + c) & (H/2 + c)kda_p + a_p & (H/2 + c)kda_- + a_- & 0 \\ 0 & -b_+ & -b_- & 1 \\ 0 & -(H/2 - c)kdb_+ + b_+ & -(H/2 - c)kdb_- + b_- & im_t(H/2 - c) \end{pmatrix},$$

with

$$\begin{aligned} a_{\pm} &= -ie^{\mp i\mu\pi} \sqrt{z_l} I_{\pm\mu}(z_l), \quad b_{\pm} = \sqrt{z_u} I_{\pm\mu}(z_u), \\ da_{\pm} &= ie^{\mp i\mu\pi} \left(\frac{I_{\pm\mu}(z_l)}{2\sqrt{z_l}} + \sqrt{z_m} \frac{dI_{\pm\mu}}{dz} \Big|_{z_l} \right), \quad db_{\pm} = \frac{I_{\pm\mu}(z_u)}{2\sqrt{z_u}} + \sqrt{z_u} \frac{dI_{\pm\mu}}{dz} \Big|_{z_u}, \\ z_l &= k(H/2 + c), \quad z_u = k(H/2 - c), \end{aligned}$$

if $|c| < H/2$ or

$$\begin{aligned}
a_{\pm} &= \sqrt{z_l} I_{\pm\mu}(z_l) , \quad b_{\pm} = \sqrt{z_u} I_{\pm\mu}(z_u), \\
da_{\pm} &= \left(\frac{I_{\pm\mu}(z_l)}{2\sqrt{z_l}} + \sqrt{z_l} \frac{dI_{\pm\mu}}{dz} \Big|_{z_l} \right) , \quad db_{\pm} = \frac{I_{\pm\mu}(z_u)}{2\sqrt{z_u}} + \sqrt{z_u} \frac{dI_{\pm\mu}}{dz} \Big|_{z_u}, \\
z_l &= -k(H/2 + c) , \quad z_u = k(H/2 - c),
\end{aligned}$$

otherwise. The amplitudes are then given by the solution to (A1).

On the other hand, the discrete spectrum of \mathbf{A} is obtained by the complex roots of

$$\det(\mathbf{B}(c)) = 0. \tag{A2}$$

The values of c satisfying (A2) are calculated iteratively using a two-dimensional secant method. For the values of k and Ri considered in section 3, no such solutions were found. That is, there are no discrete modes of \mathbf{A} and its spectrum is continuous consisting only of singular non-orthogonal modes.

REFERENCES

- Baines, P. G. and H. Mitsudera, 1994: On the mechanism of shear flow instabilities. *J. Fluid Mech.*, **276**, 327–342.
- Bretherton, F. P., 1966a: Baroclinic instability and the short wave cut-off in terms of potential vorticity. *Quart. J. Roy. Meteor. Soc.*, **92**, 335–345.
- Bretherton, F. P., 1966b: The propagation of groups of internal gravity waves in a shear flow. *Quart. J. Roy. Meteor. Soc.*, **92**, 466–480.
- Case, K. M., 1960: Stability of an idealized atmosphere. I. Discussion of results. *Phys. Fluids*, **3**, 149–154.
- Davies, H. C. and C. H. Bishop, 1994: Eady edge waves and rapid development. *J. Atmos. Sci.*, **51**, 1930–1946.
- Dongarra, J. J., B. Straughan, and D. W. Walker, 1996: Chebyshev tau-QZ algorithm methods for calculating spectra of hydrodynamic stability problems. *J. Appl. Numer. Math.*, **22**, 399–435.
- Eltayeb, I. A. and J. F. McKenzie, 1975: Critical level behaviour and wave amplification of a gravity wave incident upon a shear layer. *J. Fluid Mech.*, **72**, 661–671.
- Farrell, B. F. and P. J. Ioannou, 1993: Transient development of perturbations in stratified shear flow. *J. Atmos. Sci.*, **50**, 2201–2214.

- Farrell, B. F. and P. J. Ioannou, 1996: Generalized stability theory. Part I: Autonomous operators. *J. Atmos. Sci.*, **53**, 2025–2040.
- Harnik, N. and E. Heifetz, 2007: Relating over-reflection and wave geometry to the counter propagating Rossby wave perspective: toward a deeper mechanistic understanding of shear instability. *J. Atmos. Sci.*, **64**, 2238–2261.
- Harnik, N., E. Heifetz, O. M. Umurhan, and F. Lott, 2008: A buoyancy-vorticity wave interaction approach to stratified shear flow. *J. Atmos. Sci.*, **65**, 2615–2630.
- Hartman, R. J., 1975: Wave propagation in a stratified shear flow. *J. Fluid Mech.*, **71**, 89–104.
- Heifetz, E. and J. Methven, 2005: Relating optimal growth to counterpropagating Rossby waves in shear instability. *Phys. Fluids*, **17**, 064 107.
- Hoskins, B. J., M. E. McIntyre, and A. W. Robertson, 1985: On the use and significance of isentropic potential vorticity maps. *Quart. J. Roy. Meteor. Soc.*, **111**, 877–946.
- Jones, W. L., 1968: Reflexion and stability of waves in stably stratified fluids with shear flow : a numerical study. *J. Fluid Mech.*, **34**, 609–624.
- Kelvin, L., 1887: Stability of fluid motion: rectilinear motion of viscous fluid between two parallel plates. *Phil. Mag.*, **24**, 188–196.
- Lindzen, R. S., 1974: Stability of a Helmholtz profile in a continuously stratified infinite Boussinesq fluid-applications to clear air turbulence. *J. Atmos. Sci.*, **31**, 1507–1514.
- Lindzen, R. S., 1988: Instability of plane parallel shear flow (toward a mechanistic picture of how it works). *Pure Appl. Geophys.*, **126**, 103–121.

- Lindzen, R. S. and J. W. Barker, 1985: Instability and wave over-reflection in stably stratified shear flow. *J. Fluid Mech.*, **151**, 189–217.
- Lindzen, R. S. and A. J. Rosenthal, 1976: On the instability of Helmholtz velocity profiles in stably stratified fluids when a lower boundary is present. *J. Geoph. Res.*, **81**, 1561–1571.
- Lindzen, R. S. and A. J. Rosenthal, 1981: A WKB asymptotic analysis of baroclinic instability. *J. Atmos. Sci.*, **38**, 619–629.
- Lindzen, R. S. and A. J. Rosenthal, 1983: Instabilities in a stratified fluid having one critical layer. Part III: Kelvin-Helmholtz instabilities as overreflected waves. *J. Atmos. Sci.*, **40**, 530–542.
- Lindzen, R. S. and K. K. Tung, 1978: Wave overreflection and shear instability. *J. Atmos. Sci.*, **35**, 1626–1632.
- McIntyre, M. E. and M. A. Weissman, 1978: On radiating instabilities and resonant overreflection. *J. Atmos. Sci.*, **35**, 1190–1196.
- Orr, W. M. F., 1907: The stability or instability of the steady motions of a perfect liquid and of a viscous liquid. *Proc. R. Irish Acad. Ser. A*, **27**, 69–138.
- Reddy, S. C., P. J. Schmid, and D. S. Henningson, 1993: Pseudospectra of the Orr-Sommerfeld operator. *SIAM J. Appl. Math.*, **53**, 15–47.
- Rosenthal, A. J. and R. S. Lindzen, 1983a: Instabilities in a stratified fluid having one critical layer. Part I: Results. *J. Atmos. Sci.*, **40**, 509–520.

Rosenthal, A. J. and R. S. Lindzen, 1983b: Instabilities in a stratified fluid having one critical layer. Part II: Explanation of gravity wave instabilities using the concept of overreflection. *J. Atmos. Sci.*, **40**, 521–529.

Sakai, S., 1989: Rossby-Kelvin instability: a new type of ageostrophic instability caused by a resonance between Rossby waves and gravity waves. *J. Fluid. Mech.*, **202**, 149–176.

List of Figures

- 1 Velocity vertical profile given by (7) (solid line) and (10) (dashed line). It consists of a shear region bounded by two domains of uniform velocity flow. For the profile shown $H = 2$ and $V_0 = 1$. 30
- 2 Evolution of a wave packet given by (13)- (14) with central wavenumber $(k, m_0) = (0.275, -3)$ and $\delta z = 2$. Snapshot of streamfunction at $t = 0$ (panel a), $t = 120$ (panel b), $t = 340$ (panel c) and $t = 700$ (panel d). Only positive values are shown, the contour interval is 0.1 and the boundaries of the shear region are shown by the thick lines. 31
- 3 (a) Perturbation energy evolution in the lower region of uniform velocity calculated by (17). (b) Kinetic (solid line) and potential (dashed line) energy evolution within the shear layer calculated by (18) and (19) respectively. The times at which the maximum kinetic energy (340 advective time units) and the maximum potential energy (370 advective time units) are attained are noted by the dotted lines. (c) Average Reynold stress within the shear region (calculated by (20)) as a function of time. (d) Average buoyancy fluxes within the shear region (calculated by (21)) as a function of time. 32
- 4 Dispersion relation for the modes of the mean profile (10). The Reynolds and Richardson numbers are $Re = 1000$ and $Ri = 0.2$ respectively and $k = 0.275$. The small subset of modes responsible for the growth and stimulated emission of the incident wavepacket given by (13)-(14) is shown by the rectangle. 33

5 (a) Vertical structure of the streamfunction of the eigenmode with phase speed $c = -0.17 - 0.82i$. The structure is typical of the shear modes that are localized within the shear region. (b) Vertical structure of the streamfunction of the eigenmode with phase speed $c = -0.87 - 0.09i$. The structure is typical of the scattering modes that have a wavelike behavior in the far field. 34

6 (a) Structure of the streamfunction of the eigenmode of the scattering branch with the maximum projection coefficient a_i (see text for details). Only positive values are shown and the contour interval is 0.005. (b) Fourier decomposition of the eigenmode shown in (a). (c) Structure of the complex conjugate of the adjoint eigenmode with the maximum projection coefficient a_i . Streamfunction is shown as in (a) with the same contour interval. (d) Fourier decomposition of the adjoint mode shown in (c). 35

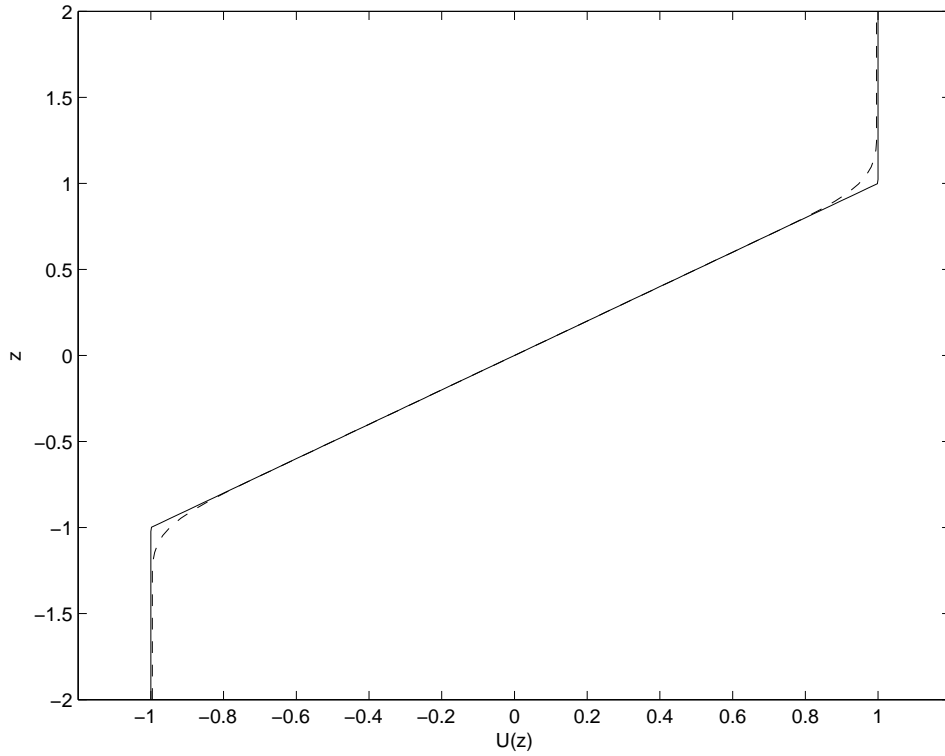


FIG. 1. Velocity vertical profile given by (7) (solid line) and (10) (dashed line). It consists of a shear region bounded by two domains of uniform velocity flow. For the profile shown $H = 2$ and $V_0 = 1$.

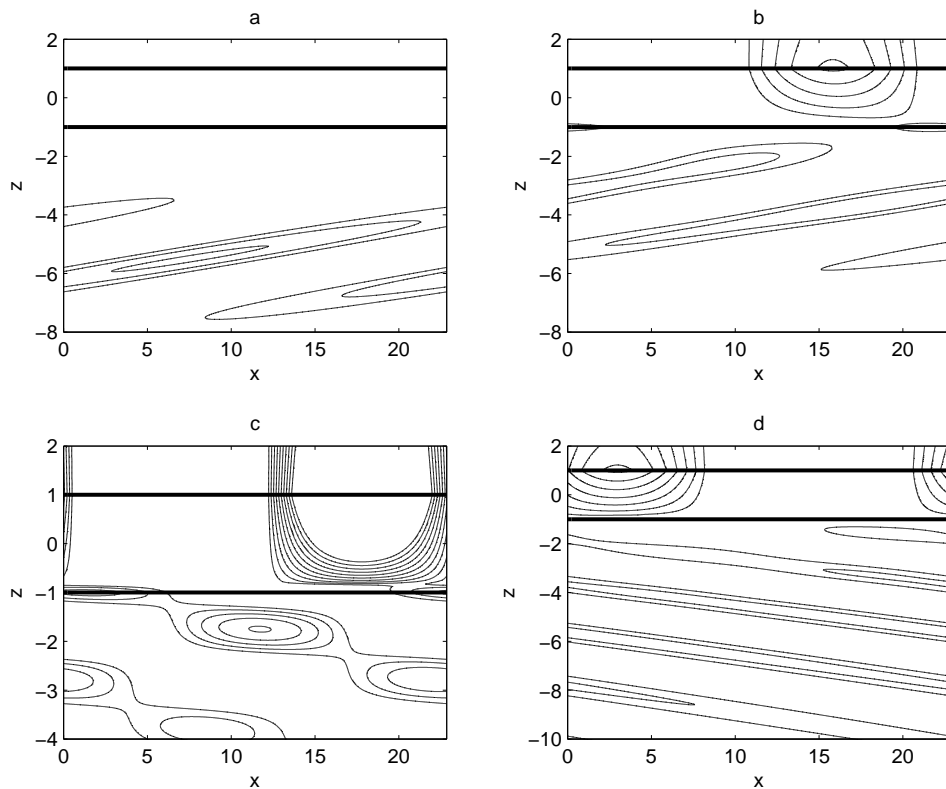


FIG. 2. Evolution of a wave packet given by (13)- (14) with central wavenumber $(k, m_0) = (0.275, -3)$ and $\delta z = 2$. Snapshot of streamfunction at $t = 0$ (panel a), $t = 120$ (panel b), $t = 340$ (panel c) and $t = 700$ (panel d). Only positive values are shown, the contour interval is 0.1 and the boundaries of the shear region are shown by the thick lines.

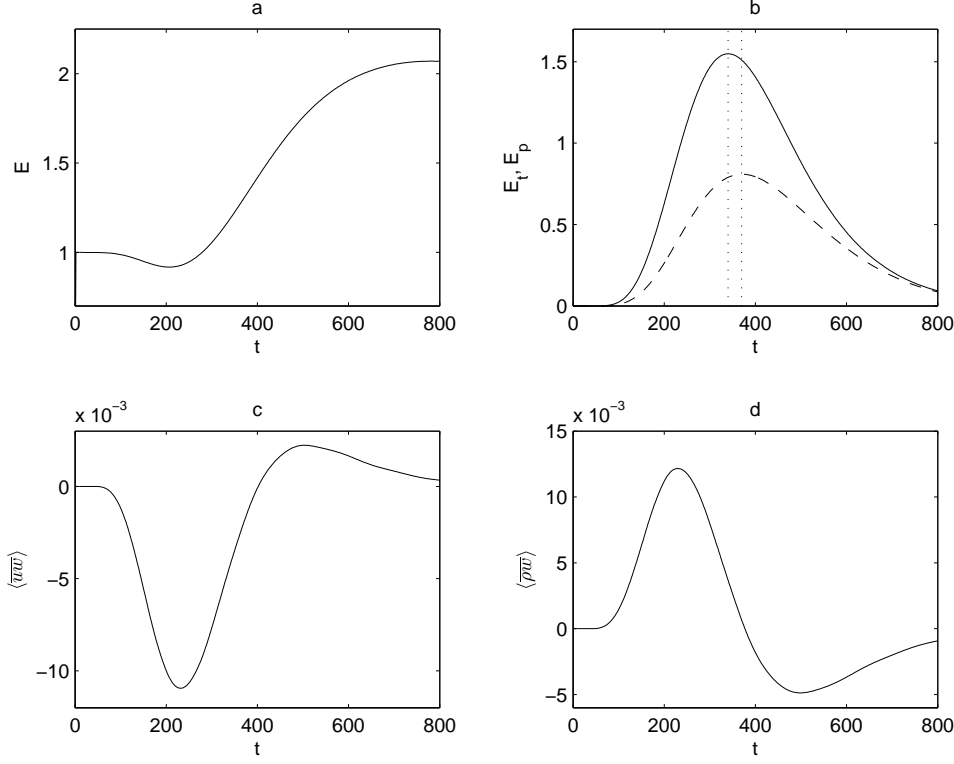


FIG. 3. (a) Perturbation energy evolution in the lower region of uniform velocity calculated by (17). (b) Kinetic (solid line) and potential (dashed line) energy evolution within the shear layer calculated by (18) and (19) respectively. The times at which the maximum kinetic energy (340 advective time units) and the maximum potential energy (370 advective time units) are attained are noted by the dotted lines. (c) Average Reynolds stress within the shear region (calculated by (20)) as a function of time. (d) Average buoyancy fluxes within the shear region (calculated by (21)) as a function of time.

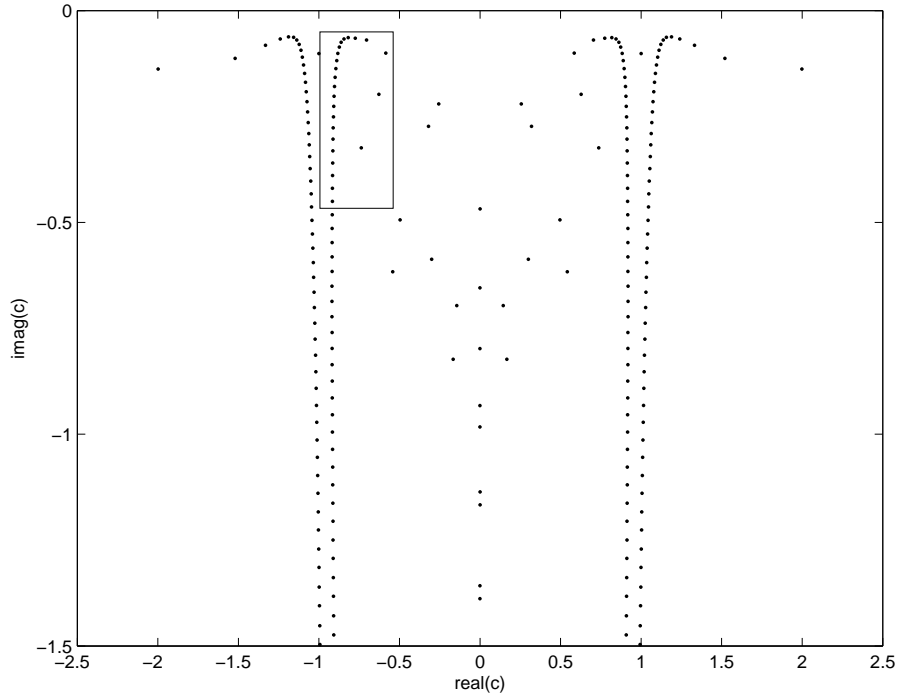


FIG. 4. Dispersion relation for the modes of the mean profile (10). The Reynolds and Richardson numbers are $Re = 1000$ and $Ri = 0.2$ respectively and $k = 0.275$. The small subset of modes responsible for the growth and stimulated emission of the incident wavepacket given by (13)-(14) is shown by the rectangle.

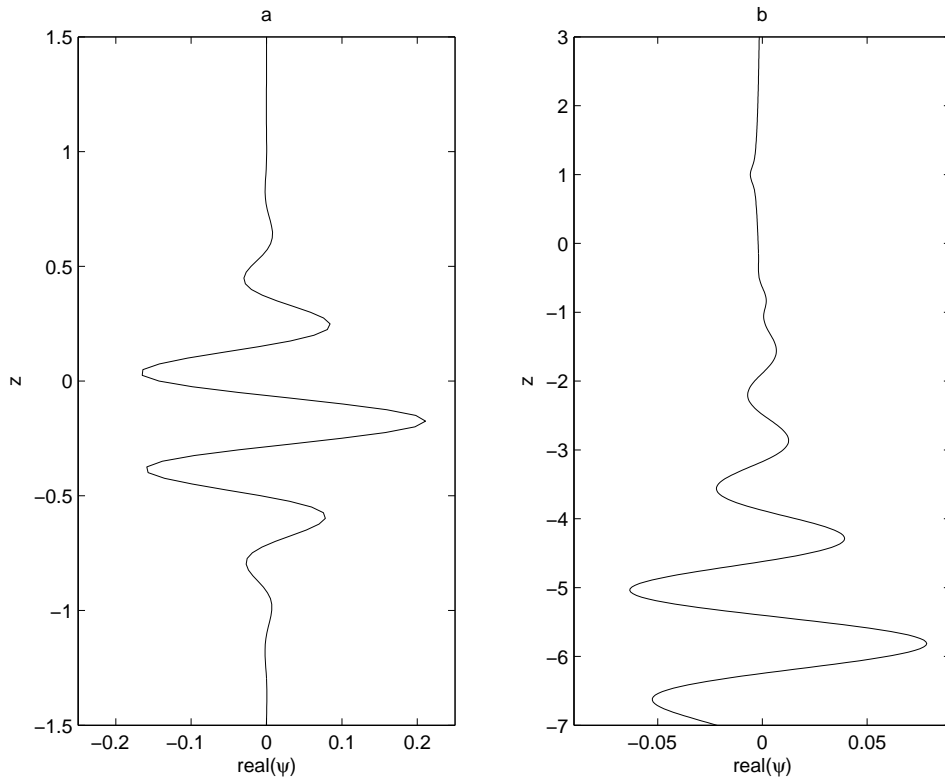


FIG. 5. (a) Vertical structure of the streamfunction of the eigenmode with phase speed $c = -0.17 - 0.82i$. The structure is typical of the shear modes that are localized within the shear region. (b) Vertical structure of the streamfunction of the eigenmode with phase speed $c = -0.87 - 0.09i$. The structure is typical of the scattering modes that have a wavelike behavior in the far field.

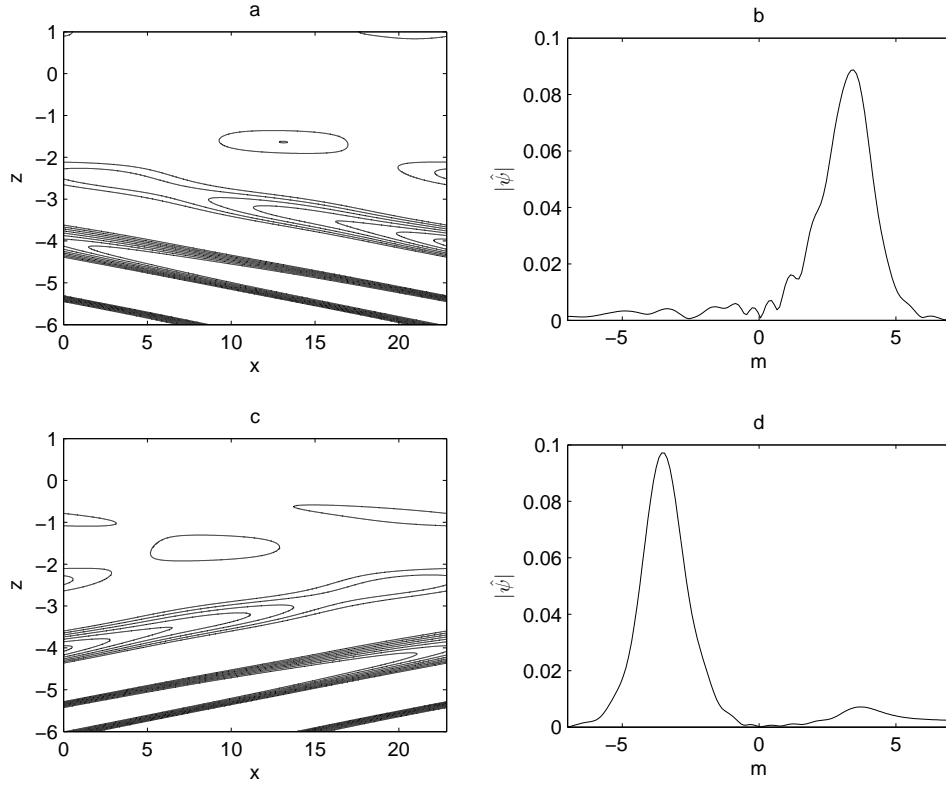


FIG. 6. (a) Structure of the streamfunction of the eigenmode of the scattering branch with the maximum projection coefficient a_i (see text for details). Only positive values are shown and the contour interval is 0.005. (b) Fourier decomposition of the eigenmode shown in (a). (c) Structure of the complex conjugate of the adjoint eigenmode with the maximum projection coefficient a_i . Streamfunction is shown as in (a) with the same contour interval. (d) Fourier decomposition of the adjoint mode shown in (c).